APPLYING UNCERTAINTY AND SENSITIVITY ON THERMAL HYDRALUIC SUBCHANNEL ANALYSIS FOR THE MULTI-APPLICATION SMALL LIGHT WATER REACTOR

A. Brigantic, W.R. Marcum *

Department of Nuclear Engineering & Radiation Health Physics, Oregon State University

3451 Jefferson Way Corvallis, OR USA

briganta@onid.oregonstate.edu, wade.marcum@oregonstate.edu

ABSTRACT

Small modular reactors (SMRs) are a recent advancement in commercial nuclear reactor design with growing interest worldwide. New SMR concepts such as the Multi-Application Small Light Water Reactor (MASLWR), must undergo a licensing processes established by the U.S. Nuclear Regulatory Commission (NRC) prior to commercial operation in the U.S. Given the lack of historical, full scale operating experience, a general uncertainty and sensitivity analysis methodology was developed to help aid SMR designs through this process. Uncertainty was quantified through the empirical cumulative distribution function (ECDF) created from a desired data set. Linear regression techniques were applied to measure sensitivity. This methodology was demonstrated through the thermal hydraulic subchannel analysis of the MASLWR concept using RELAP5-3D Version 4.0.3 and VIPRE-01 Mod 2.2.1. Twelve uncertain input parameters were selected. System response uncertainty in the minimum departure from nucleate boiling ratio (MDNBR), maximum fuel temperature, and maximum clad temperature was evaluated. These figures were shown to satisfy U.S. NRC regulatory requirements for steady state operation at the 95 percent probability and 95 percent confidence level under the evaluated conditions.

1   INTRODUCTION

Small modular reactors (SMRs) are a recent advancement in commercial nuclear reactor design with growing interest and development worldwide. Small modular reactors represent a shift in reactor design away from traditional large plants, with power production in excess of 1000 MW$_e$; SMRs are defined as power plants that produce 300 MW$_e$ or less. This decreased power production allows deployment of SMRs toward a number of potential energy markets which would have otherwise been precluded through use of traditionally sized nuclear power plants (NPPs) [1]. Included within these potential new markets is the relative locale for deployment of SMRs throughout the world. Additional benefits of SMRs include potential for increased plant security and reactor safety, particularly when coupled with passive safety systems. Due to the modular design of SMRs, it is possible to construct offsite production facilities; resulting in a different supply chain than has historically been utilized within the nuclear power industry. This alternate supply chain model has significant potential to reduce fabrication cost and time. While there presently exists a diverse range of SMR concepts currently under development, the quickest designs from a licensing and deployment perspective utilize the light water reactor technology found in many NPPs operating today. One such SMR concept is the Multi-Application Small Light Water Reactor (MASLWR), developed by Idaho National Engineering and Environmental Laboratory, Oregon State University (OSU), and NEXANT [2]. The MASLWR design utilizes natural circulation under normal operation and features passive safety systems. One tool with the potential to increase confidence in the results of thermal hydraulic analysis on the MASLWR design is that of uncertainty and sensitivity

---

* Corresponding Author

analysis. This type of analysis seeks to characterize the epistemic uncertainties associated with a mathematical system model. Epistemic uncertainty results from the inability to know an appropriate value for a quantity which otherwise assumed constant (e.g., instrumentation measurement uncertainty) [3]. Uncertainty analysis was introduced to the United States nuclear industry following changes made in 1988 to emergency core cooling system (ECCS) evaluation described in 10 CFR 50.46 [4]. These changes allowed the use of "best estimate" calculations with uncertainty analysis rather than the conservative 10 CFR 50 Appendix K methods which had been used until that time [4]. While uncertainty analysis was first introduced for ECCS calculations, the analysis methods themselves can be applied to any system model where epistemic uncertainty exists. Uncertainty analysis specifically seeks to characterize the total uncertainty found in a system response, while sensitivity analysis seeks to identify how much influence each individual, independent parameter has on a system response.

The objective of this study is to use the thermal hydraulic codes RELAP5-3D and VIPRE-01 to perform a subchannel analysis on the MASLWR under a prescribed set of operating conditions while performing a comprehensive uncertainty analysis. Both quantitative and qualitative comparisons of the results between RELAP5-3D and VIPRE-01 will be made.

2   MODELS & METHOD

A model of the MASLWR prototypical core geometry was developed using two unique codes – RELAP5-3D Version 4.0.3 and VIPRE-01 Mod 2.2.1. A selection of uncertainty analysis methodologies has been applied to thermal hydraulic calculations performed with these models and is detailed herein. The MASLWR core models in RELAP5-3D and VIPRE-01 have been designed as similar as possible. The development of the model geometry and boundary condition inputs between the two codes are analogous to one another, unless explicitly detailed hereinafter. Therefore, it is expected that any discrepancies found during uncertainty and sensitivity analysis result from differences between RELAP5-3D and VIPRE-01 themselves.

2.1   RELAP5-3D Model

A simplified core model is built from the MASLWR prototypical core. A simplified model is desirable given the relatively large number of data samples required for uncertainty analysis. Based on the core design shown in Figure 1(a) being geometrically symmetric, one-quarter of the core is modeled (Figure 1(b)), note that this is similar in model configuration to previous studies which have modeled the MASLWR core.

Because the premise of this study supports the safety basis of the MASLWR design, it is desirable to clearly and comprehensively understand phenomenon which are characteristic within the most limiting conditions of the reactor core; that is, the location within the core which produce the most extreme fluid conditions, referred to hereinafter as the 'hot channel' (e.g. low flow in combination with high heat flux and equilibrium quality). A lumped channel approach is used to model axial flow paths through the core. In order to maintain relatively high geometric resolution of the hot channel, a five by five (5x5) subchannel section is defined with the hot channel located at the center. This 5x5 section is placed in assembly A411 shown in Figure 1(a). Because the radial power profile applied in this study takes a maximum value in the core center, the center assembly is considered a conservative location for the hot channel to reside. Subchannels surrounding this section are lumped into geometric volumes that increase in physical size as they increase in distance from the 5 by 5 section of interest. Based on recommendations from the VIPRE-01 user's manual, channels are lumped such that the area increase is not greater than approximately one order of magnitude between adjacent volumes. Assemblies A412, A413, A511, A512, and A611 from Figure 1(a) are modeled as single channels. In total, 38 flow channels

are modeled – 25 single subchannels channels and 13 lumped channels. The numbering scheme of these channels is shown in Figure 1(b), with channel 13 representing the hot channel.
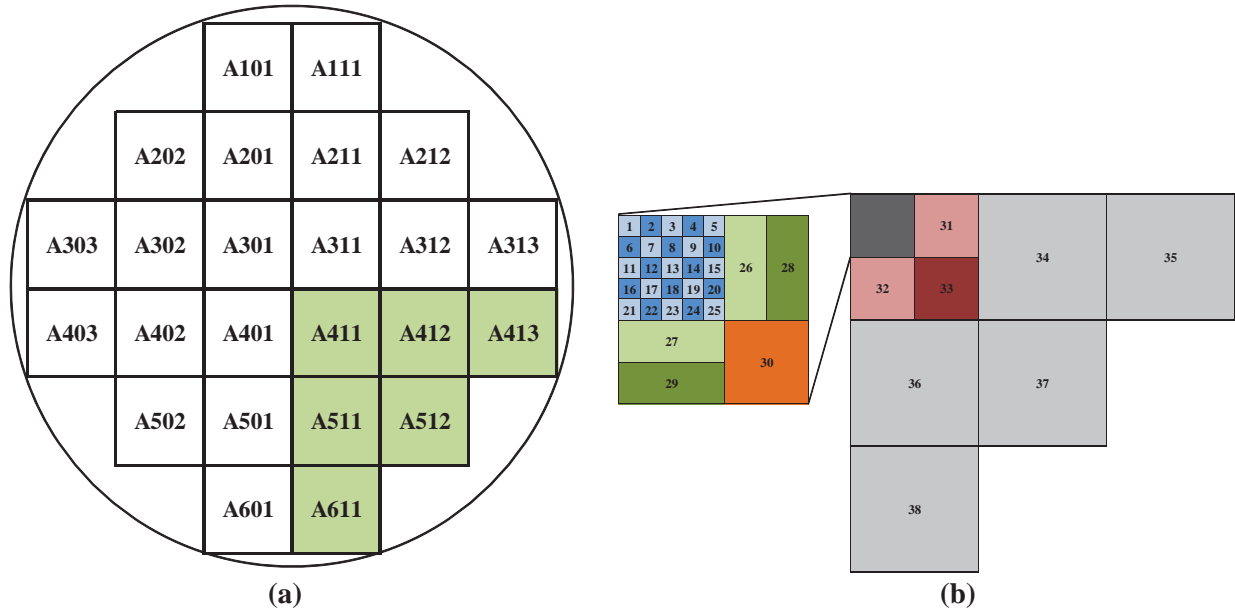

(a)

(b)

Figure 1. (a) Assemblies used in the one-quarter model and (b) Channel numbering scheme in the one-quarter MASLWR core model
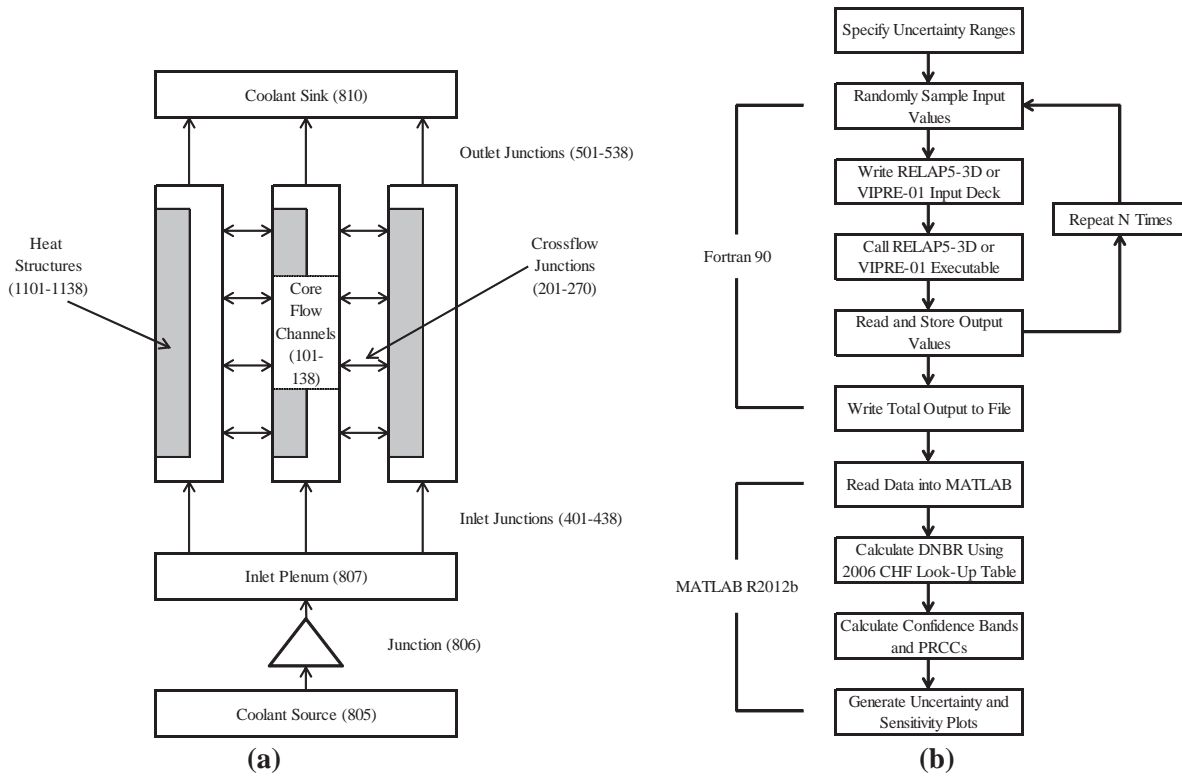

(a)

(b)

Figure 2. (a) RELAP5-3D system model and (b) overall methodology summary

A RELAP5-3D Version 4.0.3 MASLWR core model has been developed based on this lumped channel process. RELAP5-3D is a thermal hydraulic system analysis code developed at Idaho National Laboratory. RELAP5-3D was developed for light water reactor (LWR) transient analyses including LOCAs, anticipated transients without scram (ATWS), and other operational transients [5]. RELAP5-3D is a finite volume code which employs a nonhomogeneous and non-equilibrium model for two-phase flow using a partially implicit solution scheme [5].

To build a RELAP5-3D model, a series of hydraulic components are defined to construct the overall flow path, (e.g. flow through the MASLWR core subchannels). Separate heat structure components are used to model heat transfer through the fuel rods. A representative RELAP5-3D model is shown in Figure 2(a). Each case is run in transient mode for sufficient time to allow the solution to converge to steady state.

2.2   VIPRE Model

A VIPRE-01 Mod 2.2.1 MASLWR core model was developed using the same methodology as that employed to construct the RELAP5-3D model. VIPRE-01 is a thermal hydraulic subchannel analysis code originally developed by Battelle Pacific Northwest Laboratories for the Electric Power Research Institute (EPRI) in 1984 [6]. VIPRE-01 is a finite volume, three-equation code which uses the homogenous equilibrium assumption for solving two-phase flow [6].

Unlike RELAP5-3D, VIPRE-01 does not require explicit definition of component structures in order to define the system boundaries. Instead, a pre-defined geometric solution scheme is already built into VIPRE-01 based on core subchannel geometry. The user enters geometric information for N number of channels and M number of fuel rods. The user also defines which channels and fuel rods are physically linked to one another. This information was entered into VIPRE-01 following the MASLWR modeling methodology previously described. A tenth channel type was added to allow random perturbations in the hot channel geometry without affecting the remaining channels.

In addition to geometric information, the user must specify appropriate two-phase flow correlations and heat transfer correlations for VIPRE-01 to apply. Based on previous subchannel modeling of the MASLWR core, the default EPRI models were selected for the two-phase friction multiplier, subcooled void correlation, and bulk void correlation [7]. Heat transfer between the fuel rods and coolant is dependent on the local flow regime. For the single-phase region, the Dittus-Boelter correlation was applied [8]. For both the subcooled nucleate boiling and saturated nucleate boiling regions, the Chen correlation was selected [9]. The Chen correlation was selected as it is the default RELAP5-3D heat transfer correlation [5].

Unlike RELAP5-3D, VIPRE-01 has been developed with a fully implicit steady-state solution scheme. Three numerical solution methods are available: an iterative solution, a direct solution, and a recirculation solution. The recirculation solution was adapted from COBRA-WC to allow reverse and recirculating flows [6]. The recirculation solution scheme is recommended when axial flows are expected become locally small [6]. Because the MASLWR has a much smaller flow rate than traditional NPPs, the recirculation solution was used. Default convergence values for the recirculation solution were applied [10].

2.3   Figures of Merit

Uncertainty analysis requires the identification of system response variables, referred to as figures of merit (FOM), to be analyzed. There exists a vast number of potential FOM which may be extracted from the RELAP5-3D and VIPRE-01 model outputs. Relevant FOM are therefore selected based on U.S. NRC licensing requirements.

In the United States, new reactor designs are subject to the licensing approval process established by the U.S. NRC in NUREG-800. Relevant chapters to subchannel analysis include Chapter 4.2, which establishes the acceptance criteria for fuel performance characteristics, and Chapter 4.4, which establishes the acceptance criteria for thermal hydraulic calculations [11, 12]. Chapters 4.2 and 4.4 in part are designed to satisfy General Design Criteria (GDC) 10 found in Appendix A of 10 CFR Part 50 [13]. This criterion requires that specified acceptable fuel design limits are not exceeded during normal operation or Anticipated Operation Occurrences (AOOs). To ensure GDC 10 is satisfied, Chapter 4.2 requires evaluation of cladding and fuel pellet temperature to ensure failure does not occur [11]. Chapter 4.4 requires that there should be a 95 percent probability at the 95 percent confidence level that the hot rod in the core does not experience a DNB condition during normal operation or AOOs [12]. From these requirements, the following FOMs have been identified: peak cladding temperature, peak fuel temperature, and minimum departure from nuclear boiling ratio (MDNBR). These FOM will be evaluated for the hot channel in the core.

For a heated, pressurized flow channel, departure from nuclear boiling is characterized by the formation of a vapor blanket between the heated wall and the bulk liquid coolant [14]. This vapor blanket greatly increases the thermal resistance between the heated wall and the coolant, causing a temperature spike in the heated wall. This temperature spike may damage the heated structure. A departure from nuclear boiling condition occurs when the local heat flux from the heated surface exceeds the required local heat flux to produce such a vapor blanket, referred to as the critical heat flux. Local DNBR is given by

$$\text{DNBR} = q''_{CHF} \left(q''_{local} \right)^{-1} \tag{1}$$

where q''_{local} is the local heat flux through the heated wall to the coolant and q''_{CHF} is the local critical heat flux (CHF).

The mechanistic characteristics that drive CHF are complex, and many different correlations exist for different fuel geometries and flow conditions [15]. Using multiple CHF correlations to calculate DNBR would introduce additional uncertainty sources. Therefore, a single CHF correlation is selected to calculate DNBR from both RELAP5-3D and VIPRE-01 for the purpose of this study. The selected CHF correlation is the Groeneveld 2006 AECL CHF look-up tables [15]. The 2006 AECL CHF table is based on a database containing over 30,000 data points complied from numerous CHF studies. This correlation was selected given the lack of a MASLWR specific CHF correlation data and because it is often used as a benchmark for other CHF correlations. The 2006 AECL CHF look-up tables present CHF in a heated channel as a function of pressure, mass flux, equilibrium quality, and channel diameter [15]. Local CHF is calculated as

$$q''_{CHF} = f\left(P_l, G_l, X_l\right) \left(\frac{D_H}{0.8\ cm} \right)^{-\frac{1}{2}} \tag{2}$$

where P_l is the local fluid pressure, G_l is the local mass flux, and X_l is the local equilibrium quality [14].

2.4   Input Uncertainty

The International Atomic Energy Agency (IAEA) has identified three major sources of uncertainty in thermal hydraulic calculations: code or model uncertainty, representation or simulation uncertainty, and plant uncertainty [16]. In this study, code uncertainty is not considered because this requires access to the source code. As much as possible, modeling of the MASLWR core in RELAP5-3D and VIPRE-01 has been consistent in order to reduce representation uncertainty between the two codes. Therefore, plant uncertainty is evaluated herein. Herein plant uncertainty is considered as epistemic uncertainty associated

with user entered values to the RELAP5-3D and VIPRE-01 input decks. Some uncertainty methodologies, such as the code scaling, applicability, and uncertainty (CSAU) method, limit the number of uncertain parameters through expert judgment [17]. This is done through the phenomenon identification ranking table (PIRT) as developed in Step 3 of the CSAU process. Parameters are limited because the parametric response surface methodology used in CSAU is dependent on the number of parameters used. The non-parametric methods used in this study are independent of the number of uncertain parameters. However, there is still motivation to limit the number of evaluated uncertain parameters. As this is a first time uncertainty study on the MASLWR design, analysis rigor should be limited to prevent erroneous conclusions which might be drawn using too large a number of uncertain parameters. Second, the lack of MASLWR operational data within the core region (applicable to subchannel analysis) requires the use of user judgment to select and assign an uncertainty distribution to a parameter. Therefore, 12 uncertain parameters have been identified for evaluation. These parameters are considered influential on the selected figures of merit. Parameters were selected with the intention that as design and analysis maturity improves, the characterization of uncertainty sources will advance as well. These parameters were separated into two categories: plant operation uncertainty and manufacturing uncertainty. A detailed description of these parameters and their range of uncertainty is provided in reference [18].

Each uncertain input parameter must be assigned a distribution which will be propagated through the RELAP5-3D and VIPRE-01 system codes. For this study, each uncertain parameter is assigned a uniform distribution as this is considered conservative, relative to alternate commonly utilized distributions such as normal and binomial [17]. Additionally, each uncertain parameter is assumed independent from one another. In reality, it is likely some degree of dependence exists. This is especially true under natural circulation where at steady state, single phase flow rate is proportional to thermal power on the order $Q^{1/3}$. However, this assumption still allows valid comparisons between uncertainty and sensitivity results from RELAP5-3D and VIPRE-01.

The uniform distribution is considered conservative because the extreme values (i.e., the minimum and maximum values) are equally likely to occur as the nominal value. The PDF for the uniform distribution is given by [19]

$$\Pr\left[a \le X \le b\right] = f(x) = \frac{1}{b-a} \, , \tag{3}$$

where a and b are the minimum and maximum values a parameter can take. To sample from the PDF, it is converted into the cumulative probability distribution function (CDF), defined for the uniform distribution by [19]

$$\Pr\left[X \le x\right] = F(x) = \frac{x-a}{b-a} . \tag{4}$$

Solving (4) for x gives

$$x = a + F(x)\left[b-a\right], \tag{5}$$

where $F(x)$ represents the cumulative probability, ranging from 0 to 1. Simplified random sampling (SRS) is used to sample values from (5). To begin, a random number uniformly distributed between 0 and 1 is chosen. This random number is then substituted into (5) as $F(x)$. Solving (5) now gives a randomly sampled value (x), for a given uncertain input parameter. In this manner, values are uniformly sampled over the range of uncertainty for a specific parameter.

Uncertainty analysis seeks to characterize the total uncertainty in a system's response given the cumulative effect of uncertainties found in the input parameters. This study employs sampling based uncertainty analysis methods [3]. Such methods provide accurate results for relatively little development

cost. These advantages come with the caveat of requiring many data samples. Additionally, this study uses non-parametric methods. These methods do not assume a distribution shape for the final system response. Therefore, non-parametric methods are suitable for non-linear systems where it may be difficult to assign a parametric distribution. Finally, this study assumes that all output variables are either completely dependent on or independent from one another. Completely dependent variables are calculated through correlations of the remaining output variables (e.g., DNBR). Data generation required for uncertainty analysis begins through SRS of each input. Once a random value for each input is selected, these values are passed through the RELAP5-3D and VIPRE-01 system codes. Calculated values for each FOM are extracted and stored. This process continues until a sufficient number of data samples have been generated.

To quantify uncertainty in a specific FOM, the output data must be synthesized into an empirical cumulative distribution function (ECDF) and plotted with confidence bands. This method is preferred as it preserves the true distribution shape of the output FOM, where a method such as Wilks' method only expresses uncertainty as a single value. Additionally, a large number of data samples are required for both the ECDF method and sensitivity analysis. Therefore, the same set of output data samples are used for both uncertainty and sensitivity analysis.

From [20], the empirical distribution function is defined as

$$\hat{F}_n(x) = \frac{1}{n}\sum_{i=1}^{n} I(X_i \leq x),$$
(6)

where n is the total number of samples and

$$I(X_i \leq x) = \begin{cases} 1 \, if \, X_i \leq x \\ 0 \, if \, X_i \geq x \end{cases}.$$
(7)

Equation (6) can be expressed informally as

$$\hat{F}_n(x) = \frac{number \, of \, elements \, in \, the \, sample \leq x}{n}.$$
(8)

The ability of the ECDF to accurately represent the true output distribution is supported by the Glivenko-Cantelli Theorem,

$$\sup_x \left| \hat{F}_n(x) - F(x) \right| \xrightarrow{a.s.} 0,$$
(9)

which implies that the ECDF uniformly converges to the true distribution as n increases [20]. There exists an additional source of uncertainty caused by statistical variation in the output FOM data. This variation is accounted for by assigning confidence bands over the entire range of the ECDF. A confidence band is derived from the Dvoretzky-Kiefer-Wolfowitz (DKW) inequality

$$\Pr\left(\sup_x \left| F(x) - \hat{F}_n(x) \right| > \varepsilon \right) \leq 2e^{-2n\varepsilon^2}.$$
(10)

The confidence band for F is given by

$$L(x) = \max\left\{ \hat{F}_n(x) - \varepsilon_n, 0 \right\},$$
(11)

and

$$U(x) = \min\left\{ \hat{F}_n(x) + \varepsilon_n, 1 \right\},$$
(12)

where

$$\varepsilon_n = \left(\frac{1}{2n} \ln\left(\frac{2}{\alpha} \right) \right)^{\frac{1}{2}},$$
(13)

and $1-\alpha$ is the desired level of confidence [20]. $L(x)$ represents the lower confidence bound and $U(x)$ represents the upper confidence bound on the ECDF $\hat{F}_n(x)$.

2.5   Summary

The overall calculation methodology is separated into two phases: data generation and data processing. The data generation phase is performed via a Fortran 90 script. The RELAP5-3D and VIPRE-01 base models are programmed into this script. Additionally, a desired range of uncertainty for each input parameter is specified. The script then performs SRS on each input to select a random value within that range. Using these values, either a RELAP5-3D or VIPRE-01 input deck is written to a separate text file. The script uses a system command to execute a RELAP5-3D or VIPRE-01 run using the generated input deck. Once complete, the resulting output file is read and the following values for the hot channel are stored: fuel centerline temperature, clad temperature, equilibrium quality, mass flux, local pressure, and heat flux. This process is repeated until N number of data samples have been recorded. Finally, all extracted output information is written to a text file for processing.

The data processing phase is performed via MATLAB R2012b using routines from the Statistics Toolbox package. The previously generated results text file is read into MATLAB. A routine calculates CHF using linear interpolation on the 2006 AECL CHF look-up table. Confidence bands are calculated for each FOM using the DKW confidence bands. Finally, MATLAB generates plots detailing uncertainty and sensitivity results. This overall calculation methodology is presented in Figure 2(b).

3   RESULTS & DISCUSSION

Prior to discussing uncertainty results, a comparison is made between the RELAP5-3D and VIPRE-01 thermal hydraulic predictions in the hot channel. Results are plotted in the hot channel heated region as a function of vertical distance from the core inlet. Solid lines represent the mean value across all 5000 data samples for a respective axial location. Long dashed lines indicate the 5th and 95th percentiles given a 95 percent confidence interval. Short dashed lines show the absolute minimum and maximum values seen in the 5000 samples at that location. Parameters related to the FOM chosen in Chapter 4 are discussed below. Mass flux is defined as the ratio of coolant mass flow rate through a control volume to the cross sectional area of the respective control volume. In this study, focus is directed toward the limiting safety related location within the core; therefore, the hot channel assumes the control volume herein. The axial distribution of mass flux in the hot channel is presented in Figure 3(a).
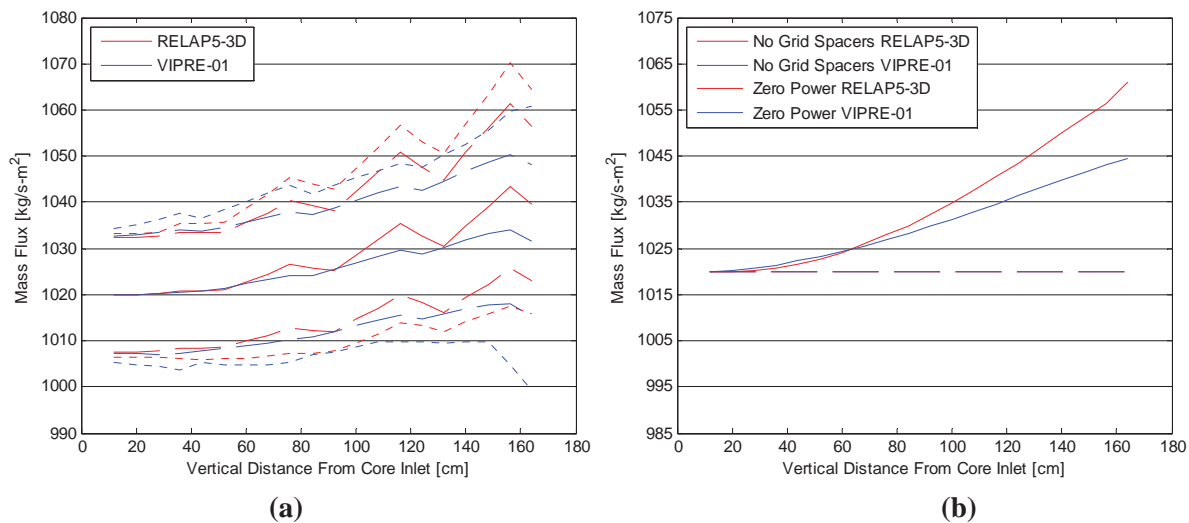

Figure 3. **(a) Mass flux through the hot channel and (b) with no grid spacers and zero power**

From Figure 3(a), RELAP5-3D and VIPRE-01 both show an increase in mass flux with an increase in vertical position within the hot channel. This general trend is expected as the coolant in the hot channel will thermally expand at a faster rate relative to coolant in surrounding channels. This creates a pressure difference which drives coolant from adjacent channels into the hot channel. The localized reduction in mass flux quantities (or 'dips') seen Figure 3(a) correspond to grid spacer locations. In an attempt to further understand the discrepancies observed in explicit mass flux values between RELAP5-3D and VIPRE-01, mass flux is calculated at nominal conditions at zero power and with grid spacers removed Figure 3(b). At zero power, RELAP5-3D and VIPRE-01 both predict a constant mass flux of 1019.9 kg/s-m^2 through the hot channel. This verifies that no relative differences between the two models are a result of geometric flow redistribution. Because the increase in mass flux is driven by the thermal expansion of the coolant, Figure 3(b) indicates that a bias exists between RELAP5-3D and VIPRE-01 fluid property calculations. Considering the case with no grid spacers, the maximum difference between RELAP5-3D and VIPRE-01 predicted mass flux is 1.68 percent. This lends further confidence toward the development of each respective model so as to allow for claims that any calculation deviations result from the computation within the codes rather than the construction of the models themselves.

The heat flux detailed herein refers to the local heat transfer rate from the clad outer surface to the coolant per unit area. The axial heat flux distribution calculated by RELAP5-3D and VIPRE-01 is shown in Figure 4(a). Heat flux calculations between the two codes are in excellent agreement. At steady state, heat flux is a function of local power and clad OD. The overlapping heat flux distributions seen in Figure 4(a) verify that local power profiles and channel geometry are correctly entered into the RELAP5-3D and VIPRE-01 models. As the axial power shape is the only non-uniform parameter which affects heat flux, the heat flux distribution is expected to follow a cosine shape. This distribution is reflected in Figure 4(a). The deflections in the upper and lower heat flux bands result from the axial power shape normalization equations described in Chapter 4. Solving these equations yield a constant local axial power factor at approximately 45 cm and 131 cm, regardless of the chosen axial peaking factor. The axial power factors at the remaining channel locations vary around these two points. A similar effect can be stated for the radial power shape as well. This effect creates a relatively flat maximum heat flux profile in the lower and upper portions of the channel, while a relatively steep maximum heat flux profile is exhibited in the channel center. The opposite trend is observed for the minimum heat flux profile.

As MDNBR was selected as a FOM, the hot channel DNBR profile is presented below. Figure 4(b) shows the local hot channel DNBR for RELAP5-3D and VIPRE-01. The DNBR was calculated during post-processing using (1). Local CHF was computed via the 2006 AECL CHF look-up table using linear interpolation between mass flux, pressure, and equilibrium quality. The DNBR distributions predicted by RELAP5-3D and VIPRE-01 are in good agreement. This is expected given the good agreement in the pressure, equilibrium quality, and heat flux results. This also indicates DNBR is much less sensitive to mass flux than the three previous quantities. Furthermore, the inverted cosine shape indicates DNBR is highly sensitive to the local heat flux distribution. This inverted cosine profile is expected from (1), where local heat flux is found in the denominator of the DNBR solution. The deflections in minimum and maximum heat flux seen in Figure 4(a) are also reflected in the minimum and maximum DNBR profiles in Figure 4(b).

The second selected FOM is maximum fuel temperature. Because this value occurs at the fuel centerline, a discussion is given regarding the observed fuel centerline temperature profile. Figure 4(c) presents fuel centerline temperature calculated by RELAP5-3D and VIPRE-01. The resulting fuel centerline temperature distributions yield nearly analogous forms. Figure 4(c) shows that the fuel centerline temperature distribution follows a cosine shape. This is expected as the only non-uniform parameter affecting fuel centerline temperature is the axial power shape. This explains the deflections seen in the minimum and maximum temperature profiles, which are also seen in Figure 4(a).
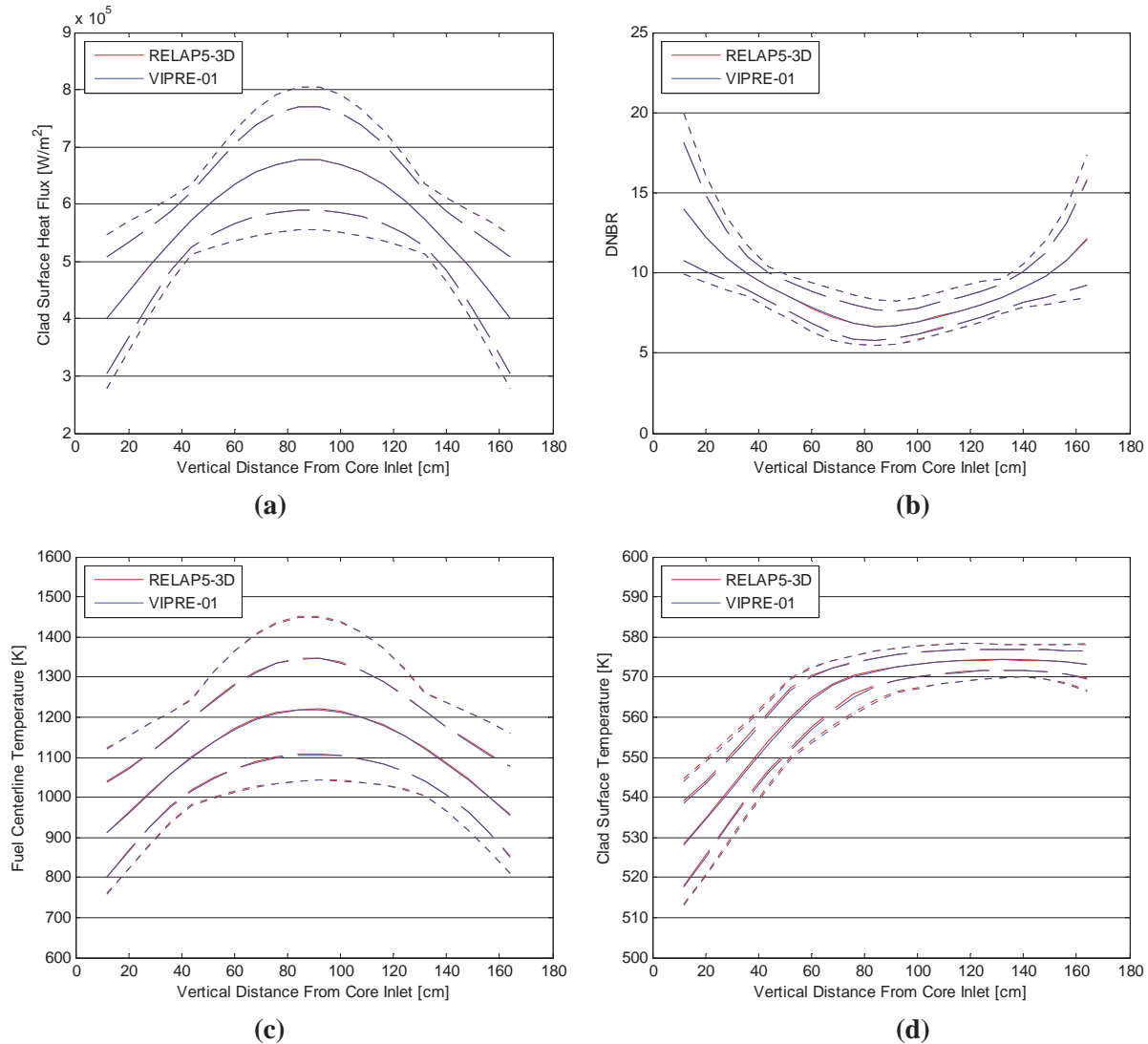
(a)

(b)

(c)

(d)

Figure 4. (a) Fuel centerline temperature, (b) DNBR, (c) clad surface heat flux, and (d) clad surface temperature

The final FOM considered is maximum clad temperature. The clad surface temperature profile is presented in order to better capture effects relating to the heat transfer coefficient between the clad and coolant. Figure 4(d) presents the clad surface temperature calculated by RELAP5-3D and VIPRE-01. In general the distributions are very similar between both codes; however, the cladding temperature in the lower region of the hot channel is predicted to be hotter in RELAP5-3D than that of VIPRE-01. As with fuel centerline temperature, it is expected that Figure 4(d) would follow a cosine shape as the only parameter affecting clad surface temperature is the axial power shape. However after initially rising, clad surface temperature remains fairly constant in the upper half of the hot channel. This indicates the assumption that clad surface temperature is independent from other output variables is invalid. Clad surface temperature is also dependent upon the bulk coolant temperature distribution and the heat transfer coefficient between the clad and coolant. Because the pressure drop across the hot channel is relatively small, the rising equilibrium quality indicates a continually rising bulk coolant temperature in the hot channel. However, the heat transfer coefficient also increases as the heat transfer regime changes from single-phase liquid to subcooled nucleate boiling at approximately 60 cm. These two facts, combined with

decreasing heat flux past the axial centerline, balance to yield a constant clad surface temperature in the upper half of the hot channel.

The selected FOMs for uncertainty analysis are MDNBR, maximum fuel temperature, and maximum clad temperature. For each of the 5000 data samples, the value of each FOM was taken as the respective minimum or maximum value seen at any axial location within the hot channel. For each FOM, an ECDF is presented through use of (6). Lower and upper confidence bounds are presented using (11) and (12) at the 95 percent confidence level (i.e. 5th and 95th percentile). As described above, an ECDF built from the MDNBR results calculated by RELAP5-3D and VIPRE-01 (Figure 5(a)).
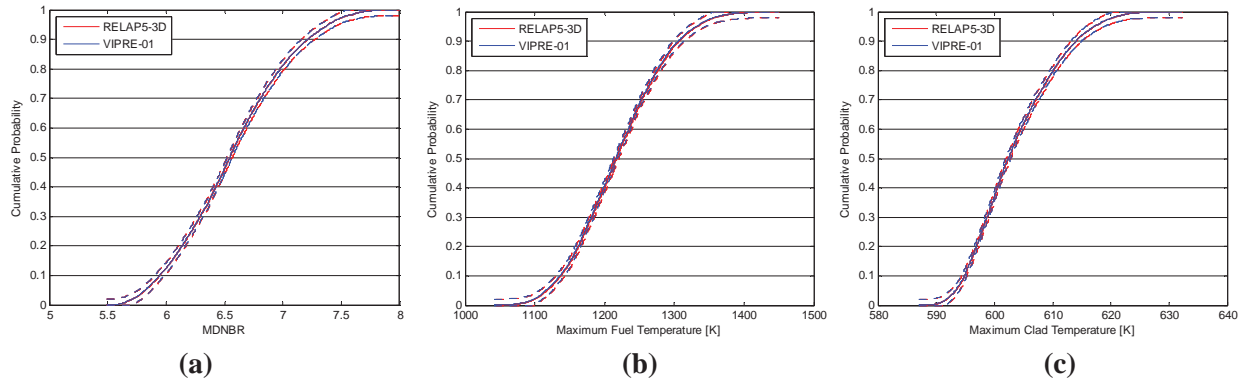

(a) (b) (c)

Figure 5. ECDF of (a) MDNBR, (b), max fuel temperature, and (c) max clad temperature

Table I. FOM percentile values from 5000 samples

FOM	Code	Min.	Percentile			Max.	Mean
			5th	50th	95th		
MDNBR [#]	RELAP5-3D	5.491	5.826	6.549	7.394	7.995	6.567
	VIPRE-01	5.488	5.822	6.547	7.390	7.996	6.566
Max fuel temp. [K]	RELAP5-3D	1044.4	1117.4	1217.3	1334.0	1450.6	1220.4
	VIPRE-01	1042.5	1115.9	1216.0	1332.6	1449.3	1219.0
Max clad temp. [K]	RELAP5-3D	587.1	593.3	602.4	617.3	632.3	603.6
	VIPRE-01	587.1	593.3	602.4	617.2	632.2	603.5

Figure 5(a) shows good agreement between the RELAP5-3D and VIPRE-01 results, as expected given the agreement shown in Figure 4(b). Key ECDF values, ignoring confidence intervals, are summarized in Table I. The span between the 5th and 95th percentiles predicted by RELAP5-3D and VIPRE-01 is 1.568 and 1.568, respectively. This correlates to a percent difference between the 5th and 95th percentiles of 23.72 percent and 23.74 percent, respectively. Acceptance criteria for MDNBR is taken from NUREG-800 Chapter 4.4, which states there should be a 95 percent probability at the 95 percent confidence level that the hot rod does not experience a DNB condition [12]. A DNB condition will occur whenever the MDNBR is less than 1.0. However, due to the uncertainty in the empirical correlations used to calculate CHF, additional margin above 1.0 is required. One common CHF correlation is the Westinghouse W-3 correlation, which has a minimum DNBR limit of 1.3 [21]. While a CHF correlation specific to the MASLWR design would likely have a different DNBR limit, a limit of 1.3 is applied in this study. To satisfy the statistical requirement in Chapter 4.4 of NUREG-800, MDNBR values are read from the upper bound of the 5th percentile in Figure 5(a). These values are 5.765 and 5.761 for RELAP5-3D and VIPRE-01 respectively. Because these values are greater than 1.3, the MASLWR design meets the DNBR safety

requirement specified in NUREG-800 Chapter 4.4 given the parameter uncertainties evaluated in this study. These MDNBR values are compared with those found in a large PWR plant, specifically the Westinghouse AP1000 design. For the AP1000, the MDNBR in a typical flow channel at nominal conditions is 2.80. While this value is approximately half that seen in Figure 5(a), it is recognized that this value was also calculated using the Westinghouse WRB-2M CHF correlation. Unlike the generalized 2006 AECL CHF look-up table, the WRB-2M correlation was designed specifically for AP1000 fuel assemblies. Therefore, core power density is also compared. The MASLWR core volume is approximated as a cylinder with an active fuel height of 160.0 cm and radius of three assembly widths, or 64.4 cm. This yields a core power density of approximately 72 kW/L at a core thermal power of 150 MW. The AP1000 has a core power density of 109.7 kW/L at a core thermal power of 3400 MW. The lower core power density seen in the MASLWR supports the higher MDNBR value compared to the AP1000.

Maximum fuel temperature is the second evaluated FOM in this study. The maximum fuel temperature is taken as the highest fuel centerline temperature seen in the hot channel for each of the 5000 data samples. Figure 5(b) presents the ECDF of the maximum fuel temperature calculated by RELAP5-3D and VIPRE-01. The distribution of results shows good agreement between the RELAP5-3D and VIPRE-01 calculations. Key ECDF values, ignoring confidence intervals, are summarized in Table I. The span between the 5th and 95th percentiles predicted by RELAP5-3D and VIPRE-01 is 216.6 K and 216.7 K, respectively. This corresponds to a percent difference between the 5th and 95th percentiles of 17.67 percent and 17.70 percent, respectively. Acceptance criteria for maximum fuel temperature is taken from NUREG-800 Chapter 4.2, which prohibits fuel centerline melting during normal operation [11]. For LWR designs, the conservatively low fuel melting temperature of 2873 K is often used. The 95 percent probability at the 95 confidence level is used to select maximum fuel temperature from Figure 5(b). This value is read from the lower bound of the 95th percentile. The RELAP5-3D and VIPRE-01 maximum fuel temperatures are 1347.3 K and 1345.6 K, respectively. Because these values are well below the 2873 K melting point, the MASLWR design satisfies the maximum fuel centerline temperature criteria established by NUREG-800 Chapter 4.2 given the parameter uncertainties evaluated in this study. The MASLWR fuel centerline temperature is compared to temperatures seen in a typical PWR. From Figure 8.22 in [14], the typical fuel rod centerline temperature at a linear power rate of 16.4 kW/m is approximately 1116 K. The core average linear power rate in the MASLWR design is 14.8 kW/m. Despite having a lower linear power rate, examining Figure 5(a) shows much of the MASWR fuel centerline temperature distribution lies above the 1116 K value; furthermore, the average maximum fuel temperature from Table I is approximately 1220 K. This higher fuel centerline temperature is credited to the different flow rates between the MASLWR design and a typical PWR. As seen in Figure 3(a), the average mass flux through the hot channel is approximately 1030 kg/s-m^2. From [14], the average subchannel mass flux for a 3400 MW PWR design is approximately 3800 kg/s-m^2, over three times higher than the MASLWR. This higher mass flux results from the forced convection used in all large PWR designs.

Maximum clad temperature is the final FOM evaluated in this study. The maximum clad temperature is taken along the inner surface of the cladding and is tabulated through identification of the highest temperature exhibited on this surface for each of the 5000 data samples. Figure 5(c) presents the ECDF of the maximum clad temperature calculated by RELAP5-3D and VIPRE-01. Figure 5(c) shows good agreement between the RELAP5-3D and VIPRE-01 results. Key ECDF values, ignoring confidence intervals, are summarized in Table I. The span between the 5th and 95th percentiles predicted by RELAP5-3D and VIPRE-01 is 24.0 K and 23.9 K, respectively. This corresponds to a percent difference between the 5th and 95th percentiles of 3.96 percent and 3.95 percent, respectively. Acceptance criteria for maximum clad temperature is taken from NUREG-800 Chapter 4.2, which requires the avoidance of clad overheating to prevent fuel failure during operation [11]. However, Chapter 4.2 also states that fuel failures associated with clad overheating will not occur as long as DNBR margin is satisfied. As previously discussed, evaluations made in this study show a DNB condition will not occur in the

MASLWR core under steady state operation. Therefore, the clad temperature requirement is satisfied according to NUREG-800 Chapter 4.2. Maximum clad temperature is of greater concern during a transient event, particularly a LOCA. In this event, clad temperature may increase rapidly due to the loss of cooling. If the zirconium cladding temperature rises too far (greater than 1477.6 K), then the cladding may undergo an exothermic reaction with water to form zirconium oxide and hydrogen gas [14]. To compare against this value, maximum clad temperatures were selected from Figure 5(c) as the lower bound of the 95th percentile. RELAP5-3D and VIPRE-01 maximum clad temperatures are determined as 619.0 K and 619.0 K, respectively. As expected for steady state operation, these values are much lower than the 1477.6 K limit.

4   SUMMARY

This study was performed to increase confidence in the thermal hydraulic safety analysis of a new reactor design through the application of uncertainty and sensitivity analysis methods. To fulfill this purpose, an uncertainty and sensitivity analysis methodology was developed and demonstrated through RELAP5-3D Version 4.0.3 and VIPRE-01 Mod 2.2.1. Several observations can be drawn from the successful application of this methodology.

First, in order to facilitate an impartial comparison between the RELAP5-3D and VIPRE-01 results, an effort was made to reduce any bias caused by the deployment of the MASLWR core model itself. Differences between the RELAP5-3D and VIPRE-01 models, specifically gap conduction, were shown to cause no bias in the final results. This claim is further supported by the overall good agreement seen between RELAP5-3D and VIPRE-01 during uncertainty and sensitivity analysis. Furthermore, it was demonstrated that differences in hot channel flow rate resulted from calculations internal to RELAP5-3D and VIPRE-01 and not the employed MASLWR model.

Knowing that any differences in results stem from the RELAP5-3D and VIPRE-01 codes themselves, a valid comparison of the uncertainty associated with each selected FOM can be made. It was shown that the RELAP5-3D and VIPRE-01 predicted hot channel MDNBR, maximum fuel temperature, and maximum clad temperature are in good agreement. Furthermore, the predicted MDNBR, maximum fuel temperature, and maximum clad temperature satisfy the acceptance criteria found in NUREG-800 under the input parameter uncertainty ranges evaluated in this study. This supports the statement that the MASLWR design is safely operable at steady state conditions.

Finally, to give further insight into the uncertainty results discussed above, several observations can be made regarding the sensitivity of each uncertain parameter on the selected FOMs. First, it is noted that the radial and axial power shapes have a high influence on all three FOMs. This is attributed to the fact that these parameters control the magnitude of the local phenomena which dictate each FOM response. Additionally, these two parameters have been assigned a relatively large range of uncertainty compared to the remaining inputs. It is also noted that certain parameters which are highly influential on some FOMs have little impact on other FOMs. These facts highlight the importance of assigning accurate uncertainty ranges to each input parameter. This also demonstrates the value of evaluating many uncertain parameters at once, versus limiting the number of parameters as done in the RS uncertainty analysis method.

5   REFERENCES

1. Cleveland, J., *Overview of Global Development of Advanced Nuclear Power Plants*. 2005, IAEA.
2. Modro, S.M., et al., *Multi-Application Small Light Water Reactor*. 2003, Idaho National Engineering and Environmental Laboratory.
3. Helton, J.C., et al., *Survey of Sampling-Based Methods for Uncertainty and Sensitivity Analysis*. 2006, Sandia National Laboratory.

4. *Best-Estimate Calculations of Emergency Core Cooling System Performance*. 1989, U.S. Nuclear Regulatory Commission.

5. *RELAP5-3D Code Manual Volume I: Code Structure, System Models and Solution Methods*. 2012, Idaho National Laboratory.

6. *Volume 1: Mathematical Modeling*. 2001, Electric Power Research Institute.

7. Mai, A.T., *Thermal Hydraulic and Fuel Performance Analysis for Innovative Small Light Water Reactor Using VIPRE-01 and FRAPCOn-3*, in *Nuclear Engineering*. 2011, Oregon State University: Corvallis.

8. Dittus, F.W. and L.M.K. Boelter, *Heat Transfer in Automobile Radiators of the Tubular Type*. 1930: University of California, Berkeley.

9. Chen, J.C., *A Correlation for Boiling Heat Transfer in Convection Flow*. Process Des. Dev., 1966. **5:322**: p. 322-329.

10. *Volume 2: User Manual*. 2001, Electric Power Research Institute.

11. NUREG-800, *U.S. Nuclear Regulatory Commission Standard Review Plan, Chapter 4.2 Fuel System Design*. 2007, U.S. Nuclear Regulatory Commission.

12. NUREG-800, *U.S. Nuclear Regulatory Commission Standard Review Plan, Chapter 4.4 Thermal and Hydraulic Design*. 2007, U.S. Nuclear Regulatory Commission.

13. *Appendix A to Part 50 - General Design Criteria for Nuclear Power Plants*, in *Code of Federal Regulations Chapter 10 Par 50*. 2014.

14. Todreas, N. and M. Kazimi, *Nuclear Systems: Thermal Hydraulic Fundamentals*. Second ed. 2012: CRC Press.

15. Groeneveld, D.C., et al., *The 2006 CHF Look-up Table*. Nuclear Engineering and Design, 2007. **237**(15): p. 1909-1922.

16. *Accident Analysis for Nuclear Power Plants*. 2002, International Atomic Energy Agency.

17. NUREG/CR-5249, *Quantifying Reactor Safety Margin*. 1989, U.S. Nuclear Regulatory Commission.

18. Brigantic, A., *Applying Uncertainty and Sensitivity on Thermal Hydraluic Subchannel Analysis for the Multi-Application Small Light Water Reactor*, in *Nuclear Engineering*. 2014, Oregon State University: Corvallis, OR. p. 127.

19. Mongomergy, D.C., G.C. Runger, and N.F. Hubele, *Engineering Statistics*. Fourth ed. 2007: John Wiley & Sons, Inc.

20. Wasserman, L., *All of Nonparametric Statistics*. 2006: Springer.

21. Lloyd, M.W. and M.A. Feltus, *Statistical Core Design Methodology Using the VIPRE Thermal-Hydraulics Code*. Annals of Nuclear Energy, 1995. **22**(8): p. 523-531.